Acta Phys. Hung. A 19/1 (2004) 000–000

HEAVY ION PHYSICS

Chiral Dynamics of Baryons in the Quark Model

Amand Faessler, Th. Gutsche, V. E. Lyubovitskij and K. Pumsa-ard

Institut für Theoretische Physik, Universität Tübingen,
Auf der Morgenstelle 14, D-72076 Tübingen, Germany

Received 1 January 2004

Abstract. We discuss recent applications of the perturbative chiral quark model (PCQM) in the analysis of the structure of baryons. The PCQM is based on an effective Lagrangian, where baryons are described by relativistic valence quarks and a perturbative cloud of Goldstone bosons as required by chiral symmetry. We discuss for example applications to electromagnetic properties of the octet baryons and σ-term physics. Furthermore, we present recent efforts to formulate and apply a manifestly Lorentz covariant chiral quark model, which is consistent with the latest developments in the baryon sector of chiral perturbation theory.

Keywords: chiral symmetry, effective Lagrangian, relativistic quark model
PACS: 12.39.Fe, 12.39.Ki, 14.20.Dh

1. Introduction

Chiral symmetry plays an important role in the low-energy domain of QCD: it governs the strong interaction between hadrons. All known low-energy approaches in the study of light hadrons have to incorporate the concept of at least an approximate chiral symmetry to get reasonable agreement with data. The concept of chiral quark models dates back to the work of the early eighties [1]-[4], where the baryon is described as a bound system of valence quarks with a surrounding Goldstone boson cloud simulating the sea-quark contributions. These models include the two main features of low-energy hadron structure, confinement, put in phenomenologically, and chiral symmetry, implemented by construction. Assuming that the valence quark content dominates the baryon, meson contributions can be treated perturbatively [1–4]. By introducing a static quark potential of general form, these quark models contain a set of free parameters characterizing the con-

1219-7580/04/ $ 20.00

finement (coupling strength) and/or the quark masses. The perturbative technique allows a fully quantized treatment of the Goldstone boson fields up to a given order in accuracy. Although formulated on the quark level, where confinement is put in phenomenologically, perturbative chiral quark models are conceptually close to chiral perturbation theory [5] on the hadron level in treating meson cloud corrections perturbatively.

As a further development of chiral quark models with a perturbative treatment of the Goldstone boson cloud we formulated the relativistic perturbative chiral quark model (PCQM) in the study of the low-energy properties of the nucleon. This model was in part applied to the electromagnetic properties of baryons [6–8] and to sigma-term physics [9, 10], which we will review in the following. We also indicate recent efforts to formulate and apply a manifestly Lorentz covariant chiral quark model, which is consistent with the latest developments in the baryon sector of chiral perturbation theory.

2. The perturbative chiral quark model

Starting point of the perturbative chiral quark model (PCQM) is an effective chiral Lagrangian describing the valence quarks of baryons as relativistic fermions moving in an external field (static potential) $V_{\rm eff}(r) = S(r) + \gamma^0 V(r)$ with $r = |\vec{x}|$, which in the SU(3) extension are supplemented by a cloud of Goldstone bosons (π, K, η). (For details see Ref. [6].) The effective Lagrangian $\mathcal{L}_{\rm eff} = \mathcal{L}_{inv} + \mathcal{L}_{\chi SB}$ of the PCQM includes a chiral invariant part $\mathcal{L}_{\rm inv}$ and a symmetry breaking term $\mathcal{L}_{\chi SB}$ (containing the mass terms for quarks and mesons):

$$\begin{aligned} \mathcal{L}_{\rm inv}(x) &= \bar{\psi}(x)[i\,\partial\!\!\!/ - \gamma^0 V(r)]\psi(x) \\ &\quad + \frac{1}{2}[D_\mu \Phi_i(x)]^2 - S(r)\bar{\psi}(x) \exp\left[i\gamma^5 \frac{\hat{\Phi}(x)}{F}\right]\psi(x), \\ \mathcal{L}_{\chi SB}(x) &= -\bar{\psi}(x)\mathcal{M}\psi(x) - \frac{B}{2}\mathrm{Tr}\left[\hat{\Phi}^2(x)\,\mathcal{M}\right], \end{aligned} \tag{1}$$

where $\hat{\Phi}(x)$ is the octet matrix of pseudoscalar mesons, D_μ is the covariant derivative; $F = 88$ MeV is the pion decay constant in the chiral limit; $\mathcal{M} = {\rm diag}\{\hat{m}, \hat{m}, m_s\}$ is the mass matrix of current quarks with the isospin averaged u-d mass $\hat{m} = 7$ MeV and $m_s = 25\hat{m}$; $B = 1.4$ GeV is the quark condensate constant.

Treating Goldstone fields as small fluctuations around the three-quark (3q) core we formulate perturbation theory in the expansion parameter $1/F$ ($F \sim \sqrt{N_c}$) and we also treat finite current quark masses perturbatively. Expanding the meson-quark interaction $\exp[i\gamma^5\hat{\Phi}(x)/F]$ up to second order in the meson field $\hat{\Phi}(x)$, all calculations are performed at one loop or at order of accuracy $o(1/F^2, \hat{m}, m_s)$. By introducing renormalized quantities, such as for quark masses and field operators, an additional set of counterterms $\delta\mathcal{L}$ has to be introduced in the Lagrangian.

The unperturbed three valence quark state is built up from the single quark wave functions obtained from the Dirac equation:

$$\Big[-i\gamma^0\vec{\gamma}\cdot\vec{\nabla}+\gamma^0 S(r)+V(r)-\mathcal{E}_\alpha\Big]\,u_\alpha(\vec{x})=0, \tag{2}$$

where $\mathcal{E}_\alpha$ is the single-quark energy. The quark wave function $u_\alpha(x)$ belongs to the basis of potential eigenstates used for the expansion of the quark field operator $\psi(x)$. We use a variational Gaussian ansatz for the quark wave function given by the analytical form:

$$u_0(\vec{x})\;=\;N\,\exp\Big[-\frac{\vec{x}^{\,2}}{2R^2}\Big]\,\left(\begin{array}{c}1\\ i\rho\,\vec{\sigma}\vec{x}/R\end{array}\right)\,\chi_s\,\chi_f\,\chi_c, \tag{3}$$

where χ_s, χ_f, χ_c are the spin, flavor and color quark wave function, respectively. The Gaussian ansatz contains two model parameters , R and ρ. The parameter ρ is fixed by the axial charge g_A of the nucleon calculated in zeroth-order (or 3q-core) approximation. The parameter R is related to the charge radius of the proton $< r_E^2 >^P_{LO}$ in the zeroth-order approximation. In our calculations we use the value g_A=1.25. Therefore, we have only one free parameter, that is R. In the numerical results [6] R is varied in the region from 0.55 fm to 0.65 fm, which corresponds to a change of $< r_E^2 >^P_{LO}$ from 0.5 to 0.7 fm^2. In the evaluation we use, if not stated otherwise, the approximation that intermediate quark lines are restricted to the ground state, that is intermediate N and Δ states occur in the one-loop terms.

3. Electromagnetic properties of baryons

As a standard application of quark models we considered the low-energy electromagnetic properties of the flavor octet baryons [6, 7]. Local gauge invariance of the electromagnetic interaction is fulfilled on the Lagrangian level by construction. Due to the noncovariant nature of the effective confinement we introduced, local gauge invariance is not necessarily fulfilled for physical amplitudes in any reference frame. Only when working in the Breit frame, nucleon matrix elements are shown to be consistent with the Ward identity.

The predictions for the magnetic moments of the baryon octet are summarized in Table 1, where the leading order valence quark contribution (LO) including corrections (renormalization of the quark wave function (NLO) and three-quark counterterms (CT)), the meson loop corrections and the total result are indicated. The mesonic contributions to the baryon magnetic moments are of the order of 20 - 40 % (except for Ξ^- they contribute only 3 %). Variations in the theoretical prediction correspond to a change in the size parameter R as discussed previously. Results for the charge radii of the baryon octet are given in Table 2. Our result for the proton and Σ^- charge radii squared are in good agreement with the experimental data. In the isospin limit the three-quark core does not contribute to the charge radii of neutral baryons. Only the meson cloud generates a nonvanishing value for the charge radii of these baryons. When we restrict the quark propagator to the ground state contribution, meson-cloud effects give a small value for

Table 1. Results for the magnetic moments μ_B of the baryon octet (in units of the nucleon magneton μ_N).

	3q [LO+NLO+CT]	Meson loops	Total	Exp [11]
μ_p	1.81 ± 0.15	0.79 ±0.12	2.60 ± 0.03	2.793
μ_n	-1.21 ± 0.10	-0.77 ± 0.12	-1.98 ± 0.02	-1.913
μ_{Σ^+}	2.24 ± 0.19	0.51 ± 0.11	2.75 ± 0.09	2.458 ± 0.010
μ_{Σ^0}	0.71 ± 0.06	0.34 ± 0.07	1.05 ± 0.01	—
μ_{Σ^-}	-0.82 ± 0.06	-0.26 ± 0.02	-1.08 ± 0.05	-1.160 ± 0.025
μ_Λ	-0.56 ± 0.06	-0.33 ± 0.09	-0.89 ± 0.03	-0.613 ± 0.004
μ_{Ξ^0}	-1.46 ± 0.14	-0.28 ± 0.11	-1.74 ± 0.03	-1.250 ± 0.014
μ_{Ξ^-}	-0.62 ± 0.07	-0.05 ± 0.07	-0.68 ± 0.01	-0.651± 0.003
$\|\mu_{\Sigma^0\Lambda}\|$	1.29 ± 0.11	0.61 ± 0.09	1.89 ± 0.01	1.61 ± 0.08

Table 2. Results for the charge radii squared $\langle r_E^2\rangle^B$ of the baryon octet (in units of fm^2).

	3q [LO+NLO+CT]	Meson loops	Total	Exp [11, 12]
$\langle r_E^2\rangle^p$	0.60 ± 0.10	0.12±0.01	0.72 ± 0.09	0.76±0.02
$\langle r_E^2\rangle^n_{\rm GS}$	0	-0.043 ± 0.004	-0.043 ± 0.004	
$\langle r_E^2\rangle^n_{\rm ES}$	0	-0.068 ± 0.013	-0.068 ± 0.013	
$\langle r_E^2\rangle^n_{\rm Full}$	0	-0.111± 0.014	-0.111 ± 0.014	-0.116±0.002
$\langle r_E^2\rangle^{\Sigma^+}$	0.67 ± 0.10	0.14 ± 0.004	0.81 ± 0.10	—
$\langle r_E^2\rangle^{\Sigma^0}$	0.038±0.010	0.012 ± 0.010	0.050 ± 0.010	—
$\langle r_E^2\rangle^{\Sigma^-}$	0.56 ± 0.10	0.15 ± 0.03	0.71± 0.07	0.61 ± 0.21
$\langle r_E^2\rangle^{\Lambda}$	0.038±0.010	0.012 ± 0.010	0.050 ± 0.010	—
$\langle r_E^2\rangle^{\Xi^0}$	0.07±0.02	0.07±0.02	0.14 ± 0.02	—
$\langle r_E^2\rangle^{\Xi^-}$	0.52 ± 0.10	0.10 ± 0.03	0.62 ± 0.07	—
$\langle r_E^2\rangle^{\Sigma^0\Lambda}$	0	0	0	—

the neutron charge radius squared. The result of the neutron charge radius can be improved by including excited states in the quark propagator. In Table 2 we explicitly indicate our results for the neutron charge radius for the different treatment of the quark propagator. The value, where the quark propagator is restricted to the ground state, is indicated by $\langle r_E^2\rangle^n$(GS). Contributions from excited states are denoted by $\langle r_E^2\rangle^n$(ES). Exemplified for the neutron charge radius, we conclude that excited state contributions can also generate sizable corrections when the LO results is vanishing.

Electromagnetic transitions of the nucleon to baryon excitations give important insight into the degrees of freedom which are relevant for the structure of baryons. From this point of view the study of the particular transition $\gamma N \to \Delta(1232)$ is sensitive to the spatial and spin structure of the involved baryons. The transverse helicity amplitudes are defined as

$$A_M = -\frac{e}{\sqrt{2\omega_\gamma}} < \Delta, s_z^{'} = M | \vec{j} \cdot \vec{\epsilon} | N, s_z = M - 1 > \qquad (4)$$

with projection $M = \frac{1}{2}, \frac{3}{2}$ and ω_γ is the energy of the photon in the rest frame of the Δ with the polarization vector $\vec{\epsilon}$. In the context of the PCQM [8] the helicity

Table 3. Results for the transverse helicity amplitudes $\gamma N \to \Delta$ at the real photon point (in units of $10^{-3}\,\mathrm{GeV}^{-1/2}$). Results for inclusion of ground (GS) and excited states (ES) in the quark propagator are indicated separately.

	$A_{1/2}(Q^2 = 0)$	$A_{3/2}(Q^2 = 0)$
GS quark propagator		
3q-core		
-LO	-69.7 ± 5.9	-120.7 ± 10.2
-NLO	-8.6 ± 1.2	-14.9 ± 2.1
Counter-term	8.2 ± 1.1	14.2 ± 1.9
Meson-cloud	-16.7 ± 2.6	-28.9 ± 4.5
Vertex-correction	-0.7 ± 0.1	-1.2 ± 0.1
Meson-in-flight	-23.0 ± 3.4	-39.8 ± 5.9
Total(GS)	-110.5 ± 0.3	-191.3 ± 0.5
ES quark propagator		
NLO	-10.3 ± 1.1	-17.8 ± 1.9
Counter-term	4.9 ± 0.6	8.5 ± 1.0
Meson-cloud	-13.5 ± 2.5	-23.4 ± 4.3
Vertex-correction	-0.7 ± 0.1	-1.2 ± 0.1
Total(ES)	-19.6 ± 3.1	-33.9 ± 5.3
Total=Total(GS)+Total(ES)	-130.1 ± 3.4	-225.2 ± 5.8
Experiment [11]	-135 ± 6	-255 ± 8

amplitudes $A_{1/2}$ and $A_{3/2}$ are evaluated at one-loop or to the order of accuracy $o(1/F^2, \hat{m}, m_s)$. At this level, which is also equivalent to $O(1/N_c)$, we obtain the naive relation $A_{3/2} = \sqrt{3} \cdot A_{1/2}$. Recently, in the framework of large-N_c [13] it was shown that the ratio $A_{3/2}/A_{1/2}$ is mostly saturated by the naive SU_6 quark model result $A_{3/2}/A_{1/2} = \sqrt{3}$. Deviations from this standard result are due to higher order corrections with $A_{3/2}/A_{1/2} = \sqrt{3} + O(1/N_c^2)$ [13]. In Table 3 we give our results for the helicity amplitudes at the real photon point, indicating separately the contributions of ground and excited states in the quark propagator. Meson cloud corrections play a decisive role in explaining the large deviation from the result of the impulse, that is three-quark core, approximation. Excited quark states in loop diagrams play an important role at the level of 15% to fully account for the measurements. Because at one-loop we work at the order of accuracy $o(1/F^2, \hat{m}, m_s)$ or equivalently at $o(1/N_c)$, a deviation from the standard ratio of $A_{3/2}/A_{1/2} = \sqrt{3}$, consistent with large-$N_c$ arguments [13] cannot be obtained. Hence, we also predict a vanishing value for the $E2/M1$ ratio.

4. Sigma-term physics

The meson-nucleon sigma-terms are fundamental parameters of low-energy hadron physics, since they provide a direct measure of the scalar quark condensates in baryons and constitute a test for the mechanism of chiral symmetry breaking. Therefore, sigma-terms pose an important test for effective quark models in the low-energy hadron sector, since these quantities are dominantly determined by the quark-antiquark sea and not by the valence quark contribution.

The scalar density operators S_i^{PCQM} $(i = u, d, s)$, relevant for the calculation of the meson-baryon sigma-terms in the PCQM, are defined as the partial derivatives of the χSB model Hamiltonian $\mathcal{H}_{\chi SB} = -\mathcal{L}_{\chi SB}$ with respect to the current quark mass m_i of i-th flavor:

$$S_i^{PCQM} \doteq \frac{\partial \mathcal{H}_{\chi SB}}{\partial m_i} = S_i^{val} + S_i^{sea}, \tag{5}$$

where $S_i^{val} \equiv \bar{q}_i q_i$ is the set of valence-quark operators and S_i^{sea} arises from the pseudoscalar meson mass term.

A perturbative evaluation of S_i^{PCQM} to one loop results in the expression for the πN sigma-term [9]:

$$\sigma_{\pi N} = \hat{m} < p|S_u^{PCQM} + S_d^{PCQM}|p >= 3\gamma\hat{m} + \sum_{\Phi=\pi,K,\eta} d_N^\Phi \cdot \Gamma(M_\Phi^2) \tag{6}$$

where the first term of the right-hand side corresponds to the valence quark, the second to the sea quark contribution. The vertex function $\Gamma(M_\Phi^2)$ is related to the partial derivative of the self-energy operator $\Pi(M_\Phi^2)$ with respect to the nonstrange current quark mass $\hat{m}$; d_N^Φ are recoupling coefficients and $\gamma = 5/8$ is a relativistic reduction factor.

In Ref. [9] we originally calculated the $\sigma_{\pi N}$ sigma-term with the quark propagator restricted to the ground state. The result we obtained there was 45 ± 5 MeV, where the variation of the value is due to a change of the range parameter R. For the central value of $R = 0.6$ fm we obtain $\sigma_{\pi N} = 42.5$ MeV, where the valence-quark contribution is $\sigma_{\pi N}^{val} = 13.1$ MeV (i.e. 1/3 of the total value) and the meson-cloud contribution is dominated by the pions with $\sigma_{\pi N}^{sea} = 29.4$ MeV (i.e. 2/3 of total value). Inclusion of the excited quark states [10] obviously does not change the result for $\sigma_{\pi N}^{val}$ but leads to an increase for $\sigma_{\pi N}^{sea}$ from 29.4 MeV to 41.6 MeV. Hence, we obtain a sizable increase of the sigma term by about 12 MeV leading to the final value of $\sigma_{\pi N} = 54.7$ MeV. The main contribution is due to pion loops, whereas kaon and eta loops are strongly suppressed. The obtained value of 54.7 MeV is still comparable to the upper limit of the canonical result 45 ± 8 MeV obtained in Ref. [14]. It is also in agreement with the result obtained in the framework of relativistic baryon ChPT up to next-next-to-leading order (NNLO) based on an extrapolation of this observable from two-flavor lattice QCD results: $\sigma_{\pi N} = 53 \pm 8$ MeV at the physical value of the pion mass [15]. Our final result is compiled as:

$$\begin{array}{lll} \sigma_{\pi N} = 54.7 \ \text{MeV}, & \sigma_{\pi N}^{val} = 13.1 \ \text{MeV}, & \sigma_{\pi N}^{sea} = 41.6 \ \text{MeV}, \\ \sigma_{\pi N}^{\pi} = 39.4 \ \text{MeV}, & \sigma_{\pi N}^{K} = 2.1 \ \text{MeV}, & \sigma_{\pi N}^{\eta} = 0.1 \ \text{MeV}, \end{array} \tag{7}$$

where the meson loop contributions are made explicit in the last line. For the slope of the scalar form factor we get:

$$\langle r^2 \rangle_N^S \doteq \langle r^2 \rangle_{\pi N}^S = -\frac{6}{\sigma_{\pi N}(0)} \frac{d\sigma_{\pi N}(Q^2)}{dQ^2}\bigg|_{Q^2=0} = 1.5 \ \text{fm}^2 \tag{8}$$

which is comparable to the model-independent prediction of Ref. [14]: $\langle r^2 \rangle_N^S \simeq 1.6$ fm^2.

The scalar nucleon form factor can be extrapolated to the time-like region $t = -Q^2$ for small t by using the linear approximation:

$$\sigma_{\pi N}(t) = \sigma_{\pi N}(0) \left(1 + \frac{1}{6} \langle r^2 \rangle_N^S \cdot t + O(t^2) \right). \tag{9}$$

Hence we obtain for the difference

$$\Delta_\sigma = \sigma_{\pi N}(2M_\pi^2) - \sigma_{\pi N}(0) = 13.8 \ \text{MeV} \tag{10}$$

which is comparable to the canonical value of $\Delta_\sigma = 15.2 \pm 0.4$ MeV deduced by dispersion-relation techniques [14] and to the results obtained in ChPT: $\Delta_\sigma = 14.0$ MeV $+2M^4\bar{e}_2$ [16] and $\Delta_\sigma = 16.9$ MeV $+2M^4\beta$ [17]. The value of the $\sigma_{\pi N}(t)$ at the Cheng-Dashen point

$$\sigma_{\pi N}(2M_\pi^2) = 68.5 \ \text{MeV} \tag{11}$$

is comparable to the upper limit (68 MeV) of the value deduced in Ref. [14], close to the central value (64 MeV) extracted from the analysis of pion-nucleon scattering data [18] and smaller than the central values of the recent analyses [19–21].

5. Covariant extension

Recently we developed a manifestly Lorentz covariant quark model [22] for the study of baryons as bound states of constituent quarks. We improved the PCQM, discussed previously, in several directions: i) the underlying model Lagrangian is fully Lorentz covariant; ii) all low-energy theorems and the infrared structure of QCD are reproduced in the extended approach due to the matching of the matrix elements to the ones derived in Chiral Perturbation Theory; iii) effects of valence quarks and meson cloud are separated in a model-independent way through the derived factorization theorem.

The approach is based on the idea that constituent quarks are treated as intermediate degrees of freedom between the current quarks (building blocks of the QCD Lagrangian) and the hadrons (building blocks of ChPT). The internal quark structure of baryons (or distribution of valence quarks) is modelled by using three-quark currents with quantum numbers of baryons and covariant baryonic wave functions. In addition to the valence quark degrees of freedom we consistently include the sea-quark effects which are parametrized by a cloud of pseudoscalar fields as dictated by chiral symmetry. Dressing of the valence quarks by a cloud of pseudoscalar mesons is based on a non-linear chirally symmetric Lagrangian. Here we follow the original ideas of Ref. [23] and include the higher-order terms in the chiral expansion. The structure of the Lagrangian is motivated by Baryon ChPT [16]. The difference is that we replace the baryon fields by the quark fields.

In a first step, this Lagrangian can be used to perform a dressing of the constituent quarks by a cloud of light pseudoscalar mesons and other heavy states using the calculational technique based on the infrared dimensional regularization of loop diagrams suggested in [16]. For the example of the electromagnetic quark transition operator the dressing by a pseudoscalar meson cloud to order $O(p^4)$ and one-loop is exemplified in Fig. 1.

For the case of the electromagnetic form factors of the nucleon, the projection of the dressed quark operators between nucleon states leads to the factorization:

$$\begin{aligned}
\langle N(p')|J^{\rm dress}_{\mu,\,\rm em}(q)|N(p)\rangle \quad &= \\
= (2\pi)^4\,\delta^4(p'-p-q) \quad & \bar u_N(p')\biggl\{\gamma_\mu\,F_1^N(q^2) + \frac{i\sigma_{\mu\nu}q^\nu}{2m_N}F_2^N(q^2)\biggr\}u_N(p) \\
= (2\pi)^4\,\delta^4(p'-p-q)\biggl\{ \quad & f_D^{ij}(q^2)\,\langle N(p')|j^{\rm bare}_{\mu,ij}(0)|N(p)\rangle \\
& + i\,\frac{q^\nu}{2\,m}\,f_P^{ij}(q^2)\,\langle N(p')|j^{\rm bare}_{\mu\nu,ij}(0)|N(p)\rangle\biggr\}\,. \qquad (12)
\end{aligned}$$

where m_N and m are the nucleon and constituent quark masses in the chiral limit; F_1^N and F_2^N are the Dirac and Pauli nucleon form factors. The effects of hadronization and confinement are contained in the matrix elements of the bare quark operators

$$j^{\rm bare}_{\mu,ij}(0) \,=\, \bar q_i(0)\,\gamma_\mu\,q_j(0) \qquad \text{and} \qquad j^{\rm bare}_{\mu\nu,ij}(0) \,=\, \bar q_i(0)\,\sigma_{\mu\nu}\,q_j(0)\,. \qquad (13)$$

The effects dictated by chiral symmetry (or chiral dynamics) are encoded in the relativistic form factors $f_D^{ij}(q^2)$ and $f_P^{ij}(q^2)$. Due to the matching of physical amplitudes to Baryon ChPT [16] we consistently reproduce all low-energy theorems and

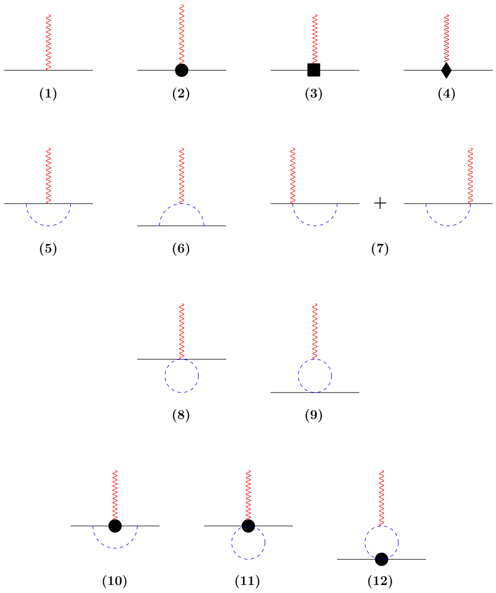

Fig. 1. Diagrams including pseudoscalar meson contributions to the electromagnetic quark transition operator up to fourth order. Solid, dashed and wiggly lines refer to quarks, pseudoscalar mesons and the electromagnetic field, respectively. Vertices denoted by a black filled circle, box and diamond correspond to insertions from the second, third and fourth chiral Lagrangian [22].

infrared properties of QCD, e.g. the leading nonanalytic (LNA) contributions to the magnetic moments μ_p and the charge $\langle r^2 \rangle_p^E$ and magnetic $\langle r^2 \rangle_p^M$ radii of nucleons. Presently, the calculation [22] of the full momentum dependence of, for example, the electromagnetic form factors relies on a full parametrization of the bare quark distributions in the nucleon and hence the particular matrix elements. To illustrate the strength of this method we indicate the results for the electric form factors of the nucleon in Fig. 2. The covariant extension of the quark model including chiral corrections to order $O(p^4)$ and one-loop serves as a basis for further investigations in topics of baryon structure, where also large momenta transfers can be studied.

Acknowledgements: This work has been supported by the Deutsche Forschungsgemeinschaft (DFG) under contracts FA 67/25-3 and GRK683. This research is also part of the EU Integrated Infrastructure Initiative Hadronphysics Project under contract number RII3-CT-2004-506078.

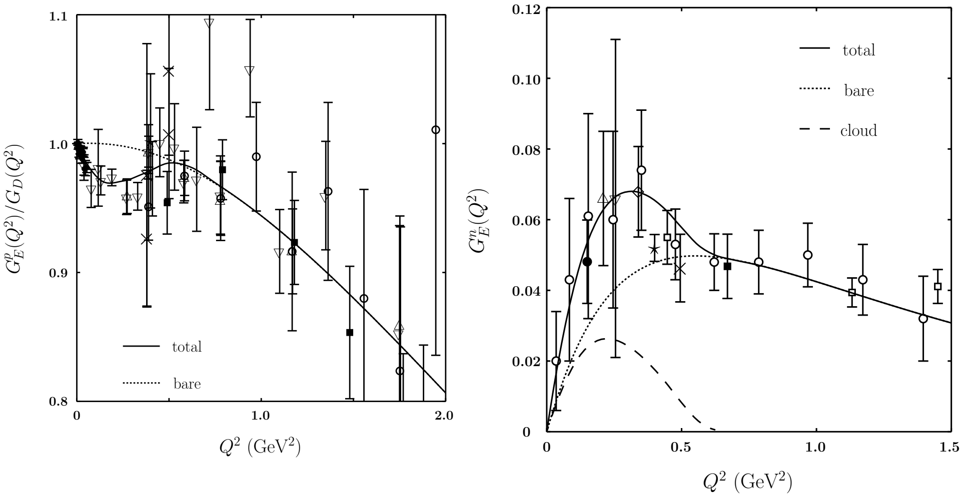

Fig. 2. Electric form factors of the nucleon: (left) Measured ratio $G_E^p(Q^2)/G_D(Q^2)$ for the proton, where G_D is the dipole form factor, (right) electric form factor of the neutron. The solid line is the total model contribution including chiral corrections and the dotted line is the bare valence quark contribution. Experimental data are taken from the compilation of Ref. [24].

References

1. S. Théberge, A. W. Thomas and G. A. Miller, Phys. Rev. D **22**, 2838 (1980); A.W. Thomas, Adv. Nucl. Phys. **13**, 1 (1984).
2. E. Oset, R. Tegen and W. Weise, Nucl. Phys. **A426**, 456 (1984); R. Tegen, Ann. Phys. **197**, 439 (1990).
3. S. A. Chin, Nucl. Phys. **A382**, 355 (1982).
4. T. Gutsche and D. Robson, Phys. Lett. **B229**, 333 (1989).
5. J. Gasser and H. Leutwyler, Ann. Phys. (N.Y.) **158**, 142 (1984); Phys. Rep. **87**, 77 (1982).
6. V. E. Lyubovitskij, T. Gutsche and A. Faessler, Phys. Rev. C **64**, 065203 (2001).
7. S. Cheedket, V. E. Lyubovitskij, T. Gutsche, A. Faessler, K. Pumsa-ard and Y. Yan, Eur. Phys. J. A **20**, 317 (2004).
8. K. Pumsa-ard, V. E. Lyubovitskij, T. Gutsche, A. Faessler and S. Cheedket, Phys. Rev. C **68**, 015205 (2003).
9. V. E. Lyubovitskij, T. Gutsche, A. Faessler and E. G. Drukarev, Phys. Rev. D **63**, 054026 (2001).
10. T. Inoue, V. E. Lyubovitskij, T. Gutsche and A. Faessler, Phys. Rev. C **69**, 035207 (2004).
11. K. Hagiwara *et al.* [Particle Data Group Collaboration], Phys. Rev. D **66**, 010001 (2002).
12. I. Eschrich *et al.* [SELEX Collaboration], Phys. Lett. B **522**, 233 (2001).

13. E. Jenkins, X. Ji, A. V. Manohar, Phys. Rev. Lett. **89**, 242001 (2002).
14. J. Gasser, H. Leutwyler and M. E. Sainio, Phys. Lett. B **253**, 252 (1991); Phys. Lett. B **253**, 260 (1991).
15. M. Procura, T. R. Hemmert and W. Weise, Phys. Rev. D **69**, 034505 (2004).
16. T. Becher and H. Leutwyler, Eur. Phys. J. C **9**, 643 (1999).
17. T. Fuchs, J. Gegelia and S. Scherer, Eur. Phys. J. A **19**, 35 (2004).
18. R. Koch, Z. Phys. C **15**, 161 (1982).
19. W. B. Kaufmann and G. E. Hite, Phys. Rev. C **60**, 055204 (1999).
20. M. G. Olsson, Phys. Lett. B **482**, 50 (2000).
21. M. M. Pavan, I. I. Strakovsky, R. L. Workman and R. A. Arndt, PiN Newslett. **16**, 110 (2002).
22. A. Faessler, T. Gutsche, V. E. Lyubovitskij, K. Pumsa-ard, [arXiv:hep-ph/0511319].
23. A. Manohar and H. Georgi, Nucl. Phys. B **234**, 189 (1984).
24. J. Friedrich and T. Walcher, Eur. Phys. J. A **17**, 607 (2003).